

Strong pairing at iron $3d_{xz,yz}$ orbitals in hole-doped BaFe_2As_2

D. V. Evtushinsky,¹ V. B. Zabolotnyy,¹ T. K. Kim,^{1,2} A. A. Kordyuk,^{1,3} A. N. Yaresko,⁴
J. Maletz,¹ S. Aswartham,¹ S. Wurmehl,¹ A. V. Boris,⁴ D. L. Sun,⁴ C. T. Lin,⁴
B. Shen,⁵ H. H. Wen,⁶ A. Varykhalov,⁷ R. Follath,⁷ B. Büchner,¹ and S. V. Borisenko¹

¹*Institute for Solid State Research, IFW Dresden, P. O. Box 270116, D-01171 Dresden, Germany*

²*Diamond Light Source Ltd., Didcot, Oxfordshire, OX11 0DE, United Kingdom*

³*Institute of Metal Physics of National Academy of Sciences of Ukraine, 03142 Kyiv, Ukraine*

⁴*Max-Planck-Institute for Solid State Research, Heisenbergstrasse 1, D-70569 Stuttgart, Germany*

⁵*Institute of Physics, Chinese Academy of Sciences, Beijing 100190, China*

⁶*National Laboratory of Solid State Microstructures and Department of Physics, Nanjing University, Nanjing 210093, China*

⁷*BESSY GmbH, Albert-Einstein-Strasse 15, 12489 Berlin, Germany*

Among numerous hypotheses, recently proposed to explain superconductivity in iron-based superconductors [1–9], many consider Fermi surface (FS) nesting [2, 4, 8, 10] and dimensionality [4, 9] as important contributors. Precise determination of the electronic spectrum and its modification by superconductivity, crucial for further theoretical advance, were hindered by a rich structure of the FS [11–17]. Here, using the angle-resolved photoemission spectroscopy (ARPES) with resolution of all three components of electron momentum and electronic states symmetry, we disentangle the electronic structure of hole-doped BaFe_2As_2 , and show that nesting and dimensionality of FS sheets have no immediate relation to the superconducting pairing. Alternatively a clear correlation between the orbital character of the electronic states and their propensity to superconductivity is observed: the magnitude of the superconducting gap maximizes at 10.5 meV exclusively for iron $3d_{xz,yz}$ orbitals, while for others drops to 3.5 meV. Presented results reveal similarities of electronic response to superconducting and magneto-structural transitions [18, 19], implying that relation between these two phases is more intimate than just competition for FS, and demonstrate importance of orbital physics in iron superconductors.

There are several experimentally established tendencies, which are followed by many representatives of iron-based family with highest T_c : presence of the electronic states with large difference in superconducting gap magnitude, often a two-gap behavior [9, 20–22], gap-to- T_c ratios much higher than the universal BCS value [9, 20, 23], correlation of T_c with anion height [24]. The phenomenology requires a large amount of input data and therefore is usually applied to a set of materials. Large diversity of electronic states at the Fermi level, found in $\text{Ba}_{1-x}\text{K}_x\text{Fe}_2\text{As}_2$ (BKFA), originally was an obstacle on the way to complete understanding of the underlying electronic structure [11, 25]. At closer look such variety of electronic states turned out to be a blessing, allowing for detailed studies of the response of different states to the superconducting transition within the same material.

The superconducting gap in BKFA was studied by means of various experimental techniques [20, 21], and vast majority of the results can be interpreted in terms of presence of comparable amount of electronic states gapped with a large gap ($\Delta_{\text{large}} = 10\text{--}11\text{ meV}$) and with a small gap ($\Delta_{\text{small}} < 4\text{ meV}$). The in-plane momentum dependence of the superconducting gap, determined in early ARPES studies, is the following: the large gap is located on all parts of the FS except for the outer hole-like FS sheet around Γ -point [25–27]. Though the crystal structure of iron-based superconductors of interest is layered, and electronic states at the Fermi level are formed mainly by the atomic orbitals of the iron planes, studying the dependence of the electronic spectrum on the out-of-plane momentum leads to quite interesting observations.

The resolution of the electronic spectra along the out-of-plane momentum is achieved in photoemission experiments via the variation of the energy of the incoming photons. Fig. 1(a) shows an energy-momentum cut capturing the Fermi crossings of the inner and outer Γ FS sheets, imaged with excitation energies in the range from 13 to 90 eV. The values of the superconducting gap were determined from the fit of the integrated energy distribution curves (IEDC) to the Dynes function [26, 28]. IEDCs and fitting curves are shown in the panel (b). Upon analysis of ARPES spectra of the BKFA one unavoidably encounters a problem of additional, presumably surface-related, contributions to the signal. This issue is discussed in the Supplementary Materials, here we only note that fitting data allowed us to single out the relevant values for the gap. The derived $h\nu$ dependence is shown in Fig. 1 (c). The gap on the inner Γ -barrel varies from maximal value of $10.5 \pm 0.5\text{ meV}$, observable for $h\nu = 13, 25, 45\text{ eV}$, to the minimal value of 4.5 meV at $h\nu = 33.5\text{ eV}$. At photon energies close to 33 eV it is possible to clearly resolve two components of the inner Γ -barrel as separate features in the spectra [see Fig. 1 (a) and Fig. S2]; at 33 eV the gaps for the Γ -barrels are: 3.5 meV for the outer one, 4.5 meV for the second and 5.5 meV for the innermost.

$\Delta_{\text{large}}(h\nu)$ is quasiperiodical, shows large flat regions with magnitude close to maximal, and rather steep decreases to the minimum and steep increases back to flats, which is particularly well illustrated by the cusp around 33.5 eV. The intensity distribution in the FS map

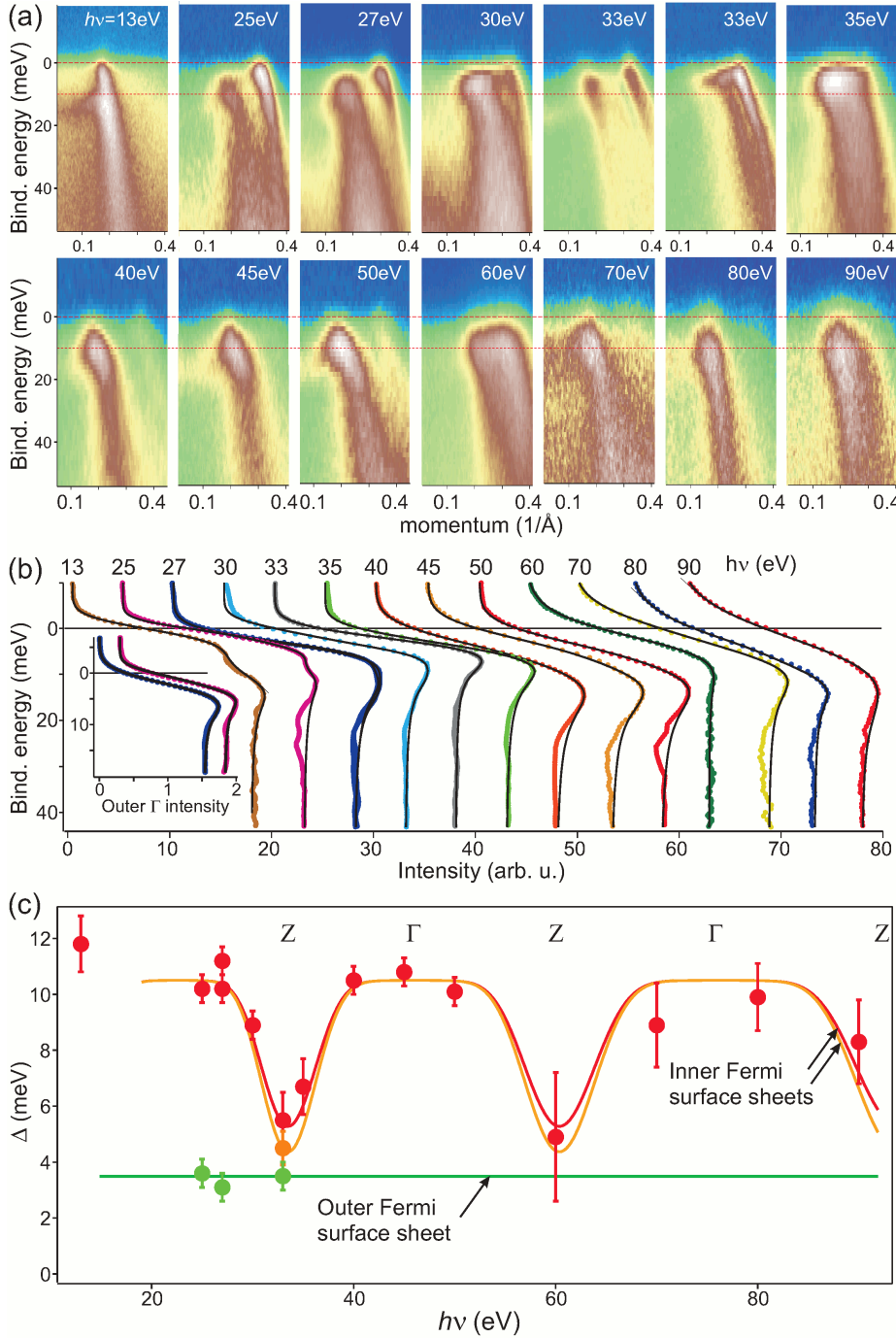


Fig.1. k_z -dependent superconducting gap at hole-like Fermi surface sheets centered at the $(k_x = 0, k_y = 0)$ point in optimally doped $\text{Ba}_{1-x}\text{K}_x\text{Fe}_2\text{As}_2$. (a) Energy-momentum cut, passing through the $(k_x = 0, k_y = 0)$ -point and capturing spectrum around Fermi crossings of Γ FS sheets, recorded at $h\nu$'s ranging from 13 to 93 eV. As discussed in the main text, the two nearly degenerate inner Γ -barrels are often not resolved. All three Γ -barrels are clearly resolved at excitation energies around the value of $h\nu = 33.5$ eV. Red dashed lines are guides to the eye, located at 0 and 10 meV binding energy. (b) Integrated energy distribution curves (IEDC) fitted to the Dynes function. (c) Values of the superconducting gaps at Γ -barrels as a function of $h\nu$. Underlying fitting curves are approximated by simple formula derived for a free-electron-like final state and inner potential of 7.6 eV. Note the large flat regions in k_z -dependence of Δ_{large} in between of cusps at $h\nu = 33.5, 60$ and 93 eV, corresponding to the variation of intensity in Fig. 1 (b). Taking into account that k_z -dependence of the gap is observed only for the inner Γ -barrels and there it possesses large flat regions, the two-gap model still can be sufficient for satisfactory interpretation of many experimental results.

(Fig. S1), also shows rather fast variations at 33.5, 60 and 93 eV, and regions with rather smooth variation of the signal in between. Interestingly, there is a rather transparent connection of such $h\nu$ -dependence of the photoemission signal to the k_z -dependence of the electronic states at the Fermi level in the band structure calculation: as seen in Fig. S3, there is a band at $(k_x = 0, k_y = 0)$, which is far above the Fermi level at $k_z = 0$ and comes down and starts to interact with two $d_{xz,yz}$ -derived hole-like bands in a rather narrow region around

$k_z = \pi$. The gap on the outer Γ -barrel, Δ_{small} , remains in the range of 3.5 ± 0.5 meV for the whole range of different k_z values [Fig. 1 (c)], i.e. is essentially k_z -independent. This behavior is inline with absence of k_z dependence of the electronic states, forming the outer Γ -barrel, in the band structure calculations (see Fig. S3).

Next we identify the orbital composition of the electronic states at the Fermi level by matching the bands, observed in the ARPES spectra of BKFA, to the bands, obtained in the band structure calculations. The origin

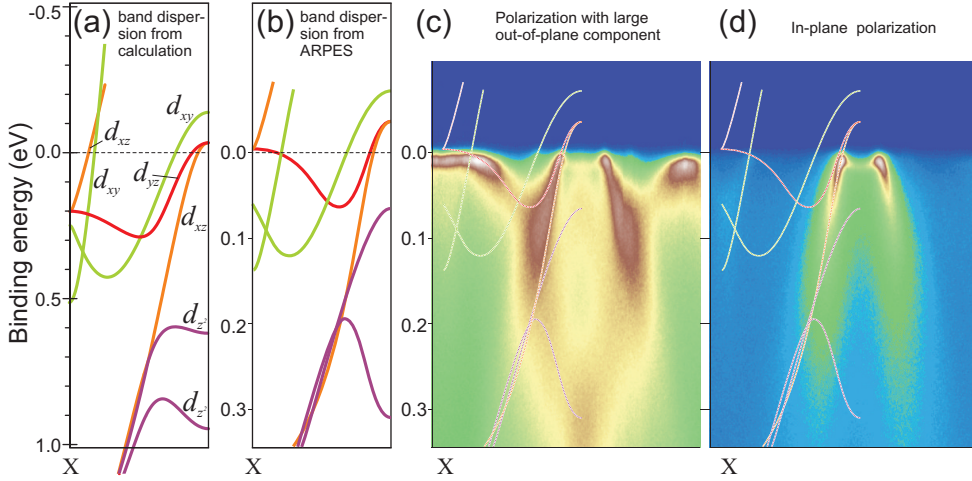


Fig.2. Comparison of the calculated band dispersion, to the band dispersion, extracted from ARPES data. (a) The calculated band dispersion. (b) The band dispersion, extracted from ARPES data, presented in panels (c,d). (c) Energy-momentum cut, passing through the ($k_x = 0$, $k_y = 0$) point, recorded at 70 eV using horizontal light polarization. (d) Same cut, recorded with vertical polarization.

of the hole-like bands in the Brillouin zone (BZ) center is clear—the outermost barrel corresponds to the band formed prevalently of iron $3d_{xy}$ orbitals, while two inner barrels consist of combinations of $3d_{xz}$ and $3d_{yz}$ orbitals [13, 14, 23, 25, 26]. The situation with the propeller-shaped bands, observed by ARPES at the BZ corner, seems to be more tricky—original FS, derived in band structure calculations, does not contain this feature [11]. On the other hand, in the calculations there is a band, situated below the Fermi level, with dispersion rather similar to the one observed experimentally for the band supporting propeller FS sheets (see Fig. 2 and Fig. S3). Therefore we employ an additional tool for identification of the electronic states—analysis of spectra, recorded with differently polarized incoming light. The grounds for such analysis stem from symmetry considerations—basing on the symmetry of the electronic wave function in the crystal and polarization direction of the incoming light, it is possible to show that the matrix element of photoemission is zero for certain experimental conditions.

Let us now consider the electronic states along ΓX line. Fig. 2(a) shows the results of calculations for this direction. We will now concentrate on the band, plotted in red; this band is composed of d_{yz} orbitals [29]. Figs. 2(c,d) show ARPES spectra, recorded in the same ΓX direction with light polarizations perpendicular (c) and parallel (d) to the ΓX . One of the most prominent changes, observed upon switching polarization is complete disappearance of the band, which was the brightest in the panel (c) and possesses dispersion very similar to the just discussed red band from the calculations. Remarkably, the d_{yz} orbital is odd with respect to the reflection in the plane containing ΓX and the direction to the detector, and therefore (due to mentioned symmetry reasons) should yield zero intensity when excited by the light polarized along ΓX . This implies that not only the d_{yz} band in the calculation possesses the dispersion similar to the dispersion of the propeller bands, derived

from ARPES, but also the strong polarization dependence, observed in ARPES, is fully consistent with the one, expected in theory. Panel (b) shows the calculated band dispersions, which are shifted in order to fit the ARPES spectra.

The last tile in the complete definition of the three-dimensional electronic structure at the Fermi level is the gap at the propeller-like bands at the BZ corner. The variations of the gap magnitude on the propellers were not observed when changing $\hbar\nu$, implying that the gap magnitude on the propeller remains ~ 10 meV for all values of k_z , in accord with previous reports [13, 14] and with little k_z -dependence of the corresponding bands in the band structure calculations.

Now, with exhaustive information on the distribution of the superconducting gap and orbital composition of the electronic states at the Fermi level at hand (Fig. 3), we see that there is a strong correlation of these two parameters. Namely, the gap is large for those and only for those states which originate purely from $d_{xz,yz}$ atomic orbitals. Indeed: (i) the gap is 3.5 meV for the outer Γ -barrel, composed of d_{xy} orbitals; (ii) the gap is 10 meV for the propellers, composed of $d_{xz,yz}$ orbitals; (iii) for the inner Γ -barrels the gap reaches 10.5 meV around $k_z = 0$, where the electronic states originate from $d_{xz,yz}$, and drops to 5 meV at $k_z = \pi$, where an admixture of d_{3z^2-1} appears; (iv) additionally, in Supplementary Materials an evidence is presented for the 3 meV gap at extra iron $3d_{3z^2-1}$ band, barely reaching the Fermi level.

The relation between the magnitude of the superconducting gap and orbital composition of the electronic state, established here on the example of $\text{Ba}_{1-x}\text{K}_x\text{Fe}_2\text{As}_2$, holds, at least partially, also for other iron-based superconductors, $\text{BaFe}_2\text{As}_{2-2x}\text{P}_{2x}$, LiFeAs , $\text{FeTe}_{1-x}\text{Se}_x$ [16, 30–32], though a thorough analysis of this issue has not been performed. An indirect confirmation for orbital dependence of the superconducting gap comes from ubiquitous observation of multigap behavior in iron-based superconductors [9, 20–22] and a

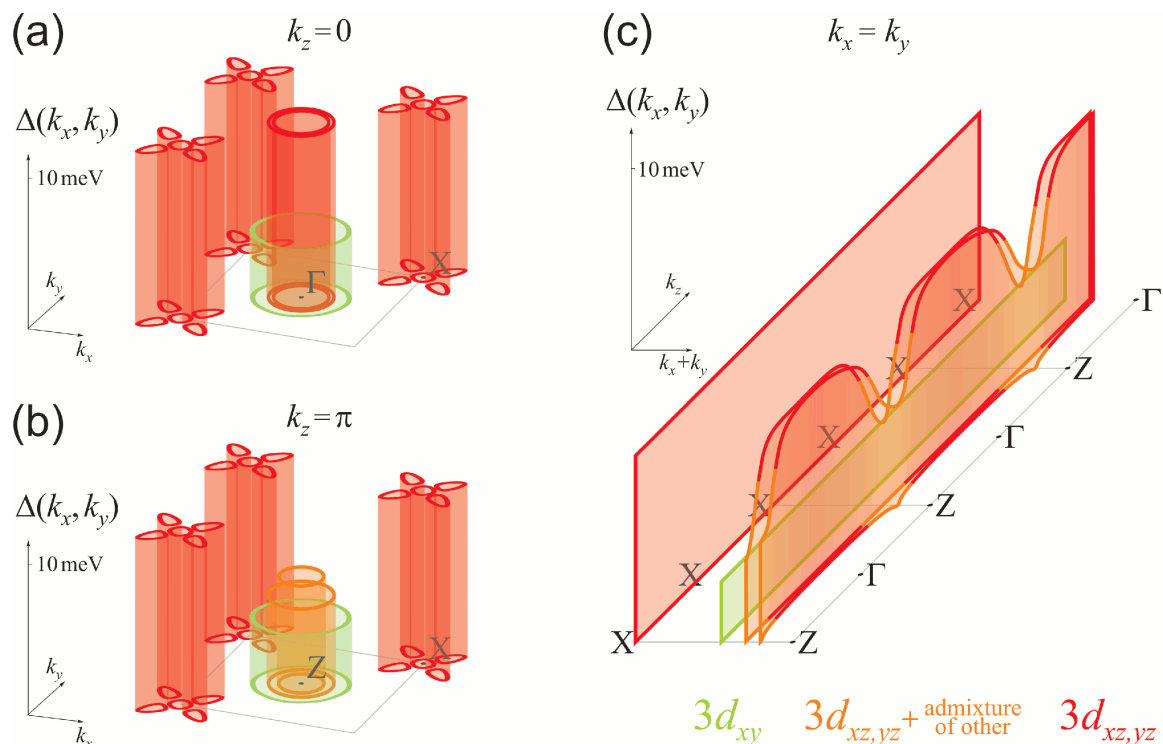


Fig.3. Three-dimensional distribution of the superconducting gap and orbital composition of the electronic states at the Fermi level. (a) Distribution of the superconducting gap (plotted as height) and distribution of the orbital composition for the states at the Fermi level (shown in color: $d_{xz,yz}$ — red, d_{xy} — green, $d_{xz,yz}$ with admixture of other orbitals — orange) as function of k_x and k_y at constant $k_z = 0$; (b) the same, only for $k_z = \pi$; (c) same distributions as function of in-plane momentum, directed along BZ diagonal, and k_z . Note unambiguous correlation between the color and height, i.e. there is strong correlation between the orbital composition and superconducting gap magnitude.

superconductivity-induced suppression of an absorption band [33].

The special role of iron $3d_{xz,yz}$ orbitals was also noticed in ARPES studies of the magneto-structural transition in the undoped and underdoped Ba-122 iron arsenides [18], implying that electronic states, which are affected most strongly by the magnetic ordering, appear to bear the largest gap in the superconducting state. This means that relation between superconductivity and magnetism in iron-based superconductors is more intimate than between phases just competing for the Fermi surface.

In summary, the momentum distribution of the superconducting gap is substantially three-dimensional and rather nontrivial. Such momentum dependence of the superconducting gap is not predicted in simple models, where the pairing strength is determined by conventional

Fermi surface nesting or dimensionality of Fermi surface sheets. Alternatively the correlation of the gap magnitude with the orbital composition of the electronic states takes place; in particular, the largest gap values were observed for iron $3d_{xz,yz}$ states.

Methods

Measurements were carried out at the 1^3 -ARPES end station at BESSY synchrotron in Berlin (Helmholtz-Zentrum für Materialien und Energie) on the single crystals of optimally doped $\text{Ba}_{1-x}\text{K}_x\text{Fe}_2\text{As}_2$ with $T_c = 38$ K [21, 34, 35]. All presented data are taken from optimally doped $\text{Ba}_{1-x}\text{K}_x\text{Fe}_2\text{As}_2$ except for the data in Fig.2(c,d), which were recorded from the optimally doped $\text{Ba}_{1-x}\text{Na}_x\text{Fe}_2\text{As}_2$ with $T_c = 34$ K [22, 36].

-
- [1] Steven A. Kivelson and Hong Yao, Iron-based superconductors: Unity or diversity? *Nature Materials* **7**, 927 (2008).
 - [2] Kazuhiko Kuroki *et.al.*, Unconventional Pairing Originating from the Disconnected Fermi Surfaces of Su-

perconducting $\text{LaFeAsO}_{1-x}\text{F}_x$. *Phys. Rev. Lett.* **101**, 087004 (2008).

- [3] A. V. Chubukov, D. V. Efremov, and I. Eremin, Magnetism, superconductivity, and pairing symmetry in iron-based superconductors. *Phys. Rev. B* **78**, 134512 (2008).

- [4] D. C. Johnston, The puzzle of high temperature superconductivity in layered iron pnictides and chalcogenides. *Advances in Physics* **59**, 803 (2010).
- [5] D. N. Basov and Andrey V. Chubukov, Manifesto for a higher T_c . *Nat. Phys.* **7**, 272 (2011).
- [6] S. Zhou, G. Kotliar, Z. Wang, Superconductivity driven by charge fluctuations in iron-pnictides. arXiv:1106.4552.
- [7] T. Imai, K. Ahilan, F. L. Ning, T. M. McQueen, and R. J. Cava, Why Does Undoped FeSe Become a High- T_c Superconductor under Pressure? *Phys. Rev. Lett.* **102**, 177005 (2009).
- [8] K. Terashima *et al.*, Fermi surface nesting induced strong pairing in iron-based superconductors. *PNAS* **106**, 7330 (2009).
- [9] F. Hardy *et al.*, Doping evolution of superconducting gaps and electronic densities of states in $\text{Ba}(\text{Fe}_{1-x}\text{Co}_x)_2\text{As}_2$ iron pnictides. *Europhys. Lett.* **91**, 47008 (2010).
- [10] J.-P. Castellán *et al.*, Effect of Fermi Surface Nesting on Resonant Spin Excitations in $\text{Ba}_{1-x}\text{K}_x\text{Fe}_2\text{As}_2$, *Phys. Rev. Lett.* **107**, 177003 (2011).
- [11] V. B. Zabolotnyy *et al.*, (π, π) electronic order in iron arsenide superconductors. *Nature (London)* **457**, 569 (2009).
- [12] A. N. Yaresko, G.-Q. Liu, V. N. Antonov, O.K. Andersen, Interplay between magnetic properties and Fermi surface nesting in iron pnictides. *Phys. Rev. B* **79**, 144421 (2009).
- [13] Y. Zhang *et al.*, Out-of-Plane Momentum and Symmetry-Dependent Energy Gap of the Pnictide $\text{Ba}_{0.6}\text{K}_{0.4}\text{Fe}_2\text{As}_2$ Superconductor Revealed by Angle-Resolved Photoemission Spectroscopy. *Phys. Rev. Lett.* **105**, 117003 (2010).
- [14] Y.-M. Xu *et al.*, Observation of a ubiquitous three-dimensional superconducting gap function in optimally doped $\text{Ba}_{0.6}\text{K}_{0.4}\text{Fe}_2\text{As}_2$. *Nat. Phys.* **7**, 198 (2011).
- [15] S. V. Borisenko *et al.*, Superconductivity without Nesting in LiFeAs . *Phys. Rev. Lett.* **105**, 067002 (2010).
- [16] H. Miao *et al.*, Isotropic superconducting gaps with enhanced pairing on electron Fermi surfaces in $\text{FeTe}_{0.55}\text{Se}_{0.45}$. arXiv:1107.0985.
- [17] Y. Zhang *et al.*, Nodeless superconducting gap in $\text{A}_x\text{Fe}_2\text{Se}_2$ ($\text{A}=\text{K}, \text{Cs}$) revealed by angle-resolved photoemission spectroscopy. *Nature Materials* **10**, 273 (2011).
- [18] M. Yi *et al.*, Symmetry-breaking orbital anisotropy observed for detwinned $\text{Ba}(\text{Fe}_{1-x}\text{Co}_x)_2\text{As}_2$ above the spin density wave transition. *PNAS* **108**, 6878 (2011).
- [19] N. Qureshi *et al.*, Local magnetic anisotropy in BaFe_2As_2 : a polarized inelastic neutron scattering study, arXiv:1201.2332.
- [20] D. V. Evtushinsky *et al.*, Momentum-resolved superconducting gap in the bulk of $\text{Ba}_{1-x}\text{K}_x\text{Fe}_2\text{As}_2$ from combined ARPES and μSR measurements. *New J. Phys.* **11**, 055069 (2009).
- [21] P. Popovich *et al.*, Specific heat measurements of $\text{Ba}_{0.68}\text{K}_{0.32}\text{Fe}_2\text{As}_2$ single crystals: evidence for a multi-band strong-coupling superconducting state. *Phys. Rev. Lett.* **105**, 027003 (2010).
- [22] A. K. Pramanik *et al.*, Multigap superconductivity in single crystals of $\text{Ba}_{0.65}\text{Na}_{0.35}\text{Fe}_2\text{As}_2$: A calorimetric investigation. *Phys. Rev. B* **84**, 064525 (2011).
- [23] D. V. Evtushinsky *et al.*, Fusion of bogoliubons in $\text{Ba}_{1-x}\text{K}_x\text{Fe}_2\text{As}_2$ and similarity of energy scales in high temperature superconductors. arXiv:1106.4584.
- [24] H. Okabe *et al.*, Pressure-induced high- T_c superconducting phase in FeSe: Correlation between anion height and T_c . *Phys. Rev. B* **81**, 205119 (2010).
- [25] H. Ding *et al.*, Observation of Fermi-surface-dependent nodeless superconducting gaps in $\text{Ba}_{0.6}\text{K}_{0.4}\text{Fe}_2\text{As}_2$. *Europhys. Lett.* **83**, 47001 (2008).
- [26] D. V. Evtushinsky *et al.*, Momentum dependence of the superconducting gap in $\text{Ba}_{1-x}\text{K}_x\text{Fe}_2\text{As}_2$. *Phys. Rev. B* **79**, 054517 (2009).
- [27] Though generally we consider essentially three-dimensional electronic structure of BKFA in this Manuscript, for the hole-like sheets in the BZ center we will use the notation of “ Γ -barrels”, stemming from two-dimensional terminology. We will also sometimes refer to the “inner” and “outer” Γ -barrels, implying that splitting of the two inner FS sheets is not principal for particular considerations.
- [28] R. C. Dynes, V. Narayanamurti, and J. P. Garno, Direct Measurement of Quasiparticle-Lifetime Broadening in a Strong-Coupled Superconductor. *Phys. Rev. Lett.* **41**, 1509 (1978).
- [29] Z. R. Ye *et al.*, Phosphor induced significant hole-doping in ferropnictide superconductor $\text{BaFe}_2(\text{As}_{1-x}\text{P}_x)_2$. arXiv:1105.5242.
- [30] S. V. Borisenko *et al.*, One-sign order parameter in iron based superconductor. *Symmetry* **4**, 251 (2012).
- [31] Y. Zhang *et al.*, Nodal superconducting gap structure in ferropnictide superconductor $\text{BaFe}_2(\text{As}_{0.7}\text{P}_{0.3})_2$. arXiv:1109.0229.
- [32] The behavior of the superconducting gap, suggesting presence of the gap nodes along k_z on the $d_{xz,yz}$ Γ -barrel, was found for the case of $\text{BaFe}_2\text{As}_{2-2x}\text{P}_{2x}$ [31]. The k_z -dependence of the gap is very reminiscent of the one, observed for $\text{Ba}_{1-x}\text{K}_x\text{Fe}_2\text{As}_2$, only with a deeper minimum at Z point. This is perfectly consistent with proposed here orbital dependence of the gap: in $\text{BaFe}_2\text{As}_{2-2x}\text{P}_{2x}$ the electronic states at Γ point exhibit stronger dependence on k_z .
- [33] A. Charnukha *et al.*, Superconductivity-induced optical anomaly in an iron arsenide, *Nature Communications* **2**, 219 (2011).
- [34] G. Sun *et al.*, Single Crystal Growth and Effect of Doping on Structural, Transport and Magnetic Properties of $\text{A}_{1-x}\text{K}_x\text{Fe}_2\text{As}_2$ ($\text{A} = \text{Ba}, \text{Sr}$)., *J. Supercond. and Nov. Magn.* **24**, 1773 (2011).
- [35] Huiqian Luo *et al.*, Growth and characterization of $\text{A}_{1-x}\text{K}_x\text{Fe}_2\text{As}_2$ ($\text{A} = \text{Ba}, \text{Sr}$) single crystals with $x = 0 - 0.4$. *Supercond. Sci. Technol.* **21**, 125014 (2008).
- [36] The electronic structures of K- and Na-doped BaFe_2As_2 are very similar. ARPES spectra of both compounds are characterized by propeller-like FS, similar magnitude and momentum distribution of the superconducting gap including very similar k_z -dependence. Possible differences between $\text{Ba}_{1-x}\text{K}_x\text{Fe}_2\text{As}_2$ and $\text{Ba}_{1-x}\text{Na}_x\text{Fe}_2\text{As}_2$ are insignificant for the presented here analysis.

Acknowledgements

We thank A.V. Chubukov for helpful discussions, to R. Hübner and R. Schönfelder for technical support.

Supplementary materials

A. k_z -resolution in ARPES on $\text{Ba}_{1-x}\text{K}_x\text{Fe}_2\text{As}_2$

In ARPES experiments one can naturally resolve the electronic spectrum along momentum components parallel to the sample surface, as k_x and k_y are conserved upon photoexcitation of electron from a crystal to vacuum. Variation of the energy of incoming photons, $h\nu$, may add the resolution of the third momentum component, k_z , if the nature of the final state is known. Within a simple model, assuming a free-electron-like final state, the dependence of k_z on $h\nu$ is rather simple [S1, S2],

$$k_z \sim \sqrt{h\nu + \text{const.}} \quad (1)$$

As was found in previous studies, the FS of BKFA consists of a propeller-like structure near the Brillouin zone corner and roundish hole-like sheets at the Γ -point [11, 26, S3]. A more precise inspection of the central region of the Brillouin zone have shown that the inner Γ -barrel is double-walled and there is another hole-like band [13, 14, 23]. Fig. S1(a) shows the distribution of the photoemission intensity at the Fermi level, superimposed by the FS contours. Fig. S1(b) shows excitation energy dependence of the intensity distribution along the line, indicated by red dotted line on the map in panel (a). Clear quasiperiodicity of the photoemission signal is observed with increasing distance between equivalent points, inline with formula (1), which provides evidence for probing different k_z at different $h\nu$ s. Additionally the magnitude of the superconducting gap, derived from experimental data changes with same quasiperiodicity in $h\nu$ (Fig. 1).

B. Spectral weight, related to $3d_{3z^2-1}$ electronic states at $(k_x = 0, k_y = 0)$

Apart from the mentioned three bands, forming quasi two-dimensional hole-like FS sheets in the center of BZ, there is also a rather diffuse intensity below the Fermi level, centered at about 100 meV binding energy [see e.g. Fig. S2 (b,d), Fig. 2 (c)]. In the band structure calculations there is a good candidate to account for this intensity—a band, formed by iron $3d_{3z^2-1}$ orbitals strongly hybridized with As p_z states, see Fig. S3 (c), Fig. 2. This band has been noticed in previous ARPES experiments on BKFA [13] and rather extensively mapped for the case of KFe_2As_2 [S4]. Panels (a) and (b) of Fig. S2 show the same energy-momentum cut, passing through the $(k_x = 0, k_y = 0)$ point, recorded with $h\nu = 33$ eV and different polarizations of the incoming light. The electronic states of interest produce much photoemission intensity for the case of horizontal polarization [see panel (b)] and are almost invisible in the vertical polarization [panel (a)]. Panel (c) shows the EDCs for $(k_x = 0, k_y = 0)$

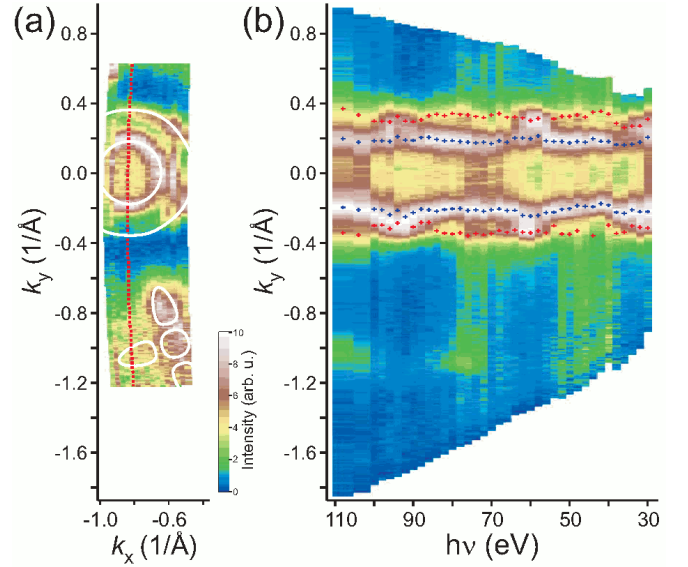


Fig. S1. ARPES with variable photon energies. (a) Fermi surface map of optimally doped $\text{Ba}_{1-x}\text{K}_x\text{Fe}_2\text{As}_2$ measured at $h\nu = 50$ eV. (b) Excitation energy map: intensity distribution along cut, indicated in panel (a) at the Fermi level (FL) was recorded using $h\nu$ in the range of 30–112 eV.

from panels (a) and (b). Not only the electronic states at higher binding energies yield more intensity when switching polarization from vertical to horizontal, but also some additional intensity appears at the Fermi level, as shown by arrows in panel (c), implying that at least some spectral weight, related to this $3d_{3z^2-1}$ band, reaches Fermi level due to self-energy broadening or/and crossing the Fermi level at some k_z values. In panel (d) we show an energy-momentum cut, recorded at 1 K with $h\nu = 34$ eV. One can notice two stripes close to the Fermi level at $(k_x = 0, k_y = 0)$: the one at higher binding energy is related to the fusion of Bogoliubov dispersion branches, observed before in BKFA [23], while the second stripe in closer vicinity to the Fermi level remained unnoticed before. In order to better visualize this spectral feature we present EDC from $(k_x = 0, k_y = 0)$ point in the panel (e). The arrows indicate the peaks—coming from the fusion of bogoliubons and the second newly detected peak. We propose that the second peak stems from a small superconducting gap opened at the discussed above electronic states, originating from a lower-lying band with $3d_{3z^2-1}$ character. From a fit to Dynes function we have determined that the magnitude of this superconducting gap is about 3 meV. Alternatively this new feature may originate from the spectral weight, related to the upper Bogoliubov dispersion branch. Though such interpretation does not explain the observed polarization dependence [Fig. S2 (a,b)] and according to simulations (not shown) requires rather large pair-breaking scattering in order to partially fill the superconducting gap, we can not rule it out at the present stage.

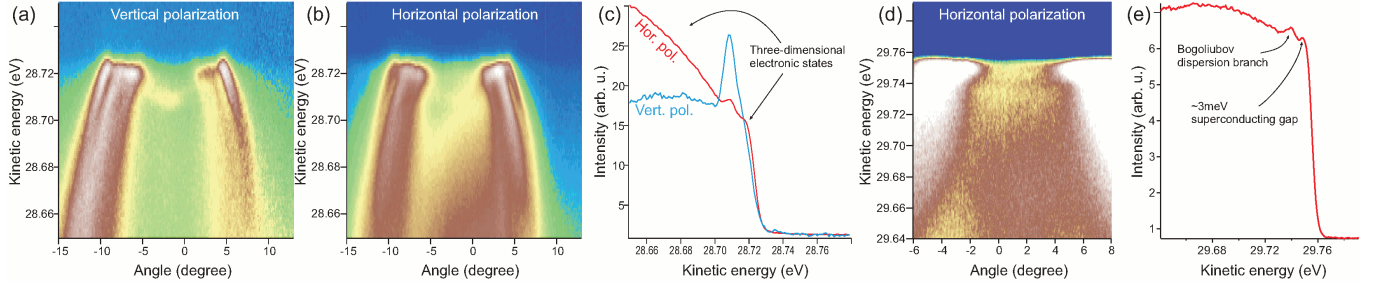


Fig. S2. Observation of the additional spectral weight from iron $3d_{3z^2-1}$ orbitals at the Fermi level and superconducting gap on it for optimally doped BKFA. (a) Energy-momentum cut, passing through the $(k_x = 0, k_y = 0)$ -point, recorded with $h\nu = 33$ meV and vertical polarization of the incoming light. (b) The same cut, recorded with horizontal polarization. (c) EDCs directly from $(k_x = 0, k_y = 0)$ -point recorded with horizontal and vertical polarizations. Comparison of EDCs recorded at different polarization suggests that spectral weight originating from three-dimensional electronic states, seen in spectrum as rather smeared intensity [see panel (b)] reaches the Fermi level. (d) Energy-momentum cut, passing through the Γ -point. (e) Γ -EDC reveals two peaks near the Fermi level: one, at binding energy about 17 meV corresponds to the observed in this compound “fusion of bogoliubons” [23], while the one closer to the Fermi level corresponds to the superconducting gap with magnitude about 3 meV.

C. Results of band structure calculations

The calculated band structure of undoped BaFe_2As_2 is presented in Fig. S3. The electronic states at the Fermi level are formed almost entirely of iron $3d$ orbitals. Panels (a)–(d) present band dispersion with superimposed circles, denoting the weight of the atomic-like states in the decomposition of the wave functions. Panel (e) presents the isoenergetic contours, obtained by cutting the calculated band dispersion at 250 meV below the Fermi level. The similarity of the four hole-like elongated ellipses at the BZ corner to the propellers, observed in FS maps, measured by ARPES, hints that the calculated and measured band structures can be matched if one slightly shifts and bends the bands. An important remark that is to be done here is that for denoting the orbital composition of the bands we use the reference frame with x and y axes directed along the diagonals of a two-dimensional Fe_2As_2 unit cell, and z directed perpendicular to the iron-arsenic layers (avoid confusion: momentum components k_x and k_y are directed parallel to the boundaries of Fe_2As_2 unit cell). The dispersion of the spectral weight near the BZ corner in the energy-momentum cut [see Fig. 2 (c)] in turn reminds the dispersion of the $3d_{xz,yz}$ band, situated right below the bottom of the electron-like pockets in the calculation [see Fig. S3 (b)]. Another characteristic feature of the calculated band structure is a strongly three-dimensional band at $(k_x = 0, k_y = 0)$ coming from high above the Fermi level as a function of k_z and starting to interact with two $3d_{xz,yz}$ bands at k_z values of about $\pi \pm \pi/4$ [see Fig. S3 (a–d)]. As already mentioned above, such behavior is consistent with rather abrupt variation of many characteristics of the photoemission spectrum in the vicinity of some values of $h\nu$ and no considerable variation for large regions in between. An independent confirmation that peculiar $h\nu$ values of 33.5, 60 and 93 eV correspond to the Z point comes from

the fitting of the $h\nu$ dependence of the superconducting gap [S5]. The detailed dependence of the electronic states of the calculated band structure on k_z is shown in Fig S3 (g): at $(k_x = 0, k_y = 0)$ the interaction of the quasi two-dimensional bands, supporting Γ FS sheets, with the mentioned band, coming from higher energies, results in the onset of the k_z dispersion and variation of the orbital composition at $k_z = \pi$.

The matrix element of a transition from an initial state u_i to a final state u_f upon action of the electromagnetic field of the incoming light can be written as

$$\int u_f^*(\mathbf{r}) \mathbf{A} \cdot \nabla u_i(\mathbf{r}) d^3\mathbf{r}, \quad (2)$$

where integration is performed over the whole coordinate space. Zero matrix element would mean that the transition does not happen, i.e. some particular electronic states do not contribute to the observed photoemission signal. Symmetry considerations reveal many cases when the matrix element is zero: e.g., if there exists such a mirror plane that the integrand is odd with respect to the corresponding reflection, the whole integral is zero. It is particularly convenient to analyze parity with respect to the plane containing both the normal to the sample surface and the momentum of photoelectron flying to the analyzer. Such an analysis has been carried out for ARPES on iron arsenides to identify the bands in the center of BZ, and in particular to resolve two closely located bands in the center of BZ [13]. In Fig. 2 (c,d) we propose a similar analysis for the energy-momentum cut passing through the BZ diagonal and cutting through all different FS sheets. For the case of the bands, formed by combination of $d_{xz,yz}$ orbitals, the orbitals lying in a plane are even with respect to reflection in it, while the ones standing “perpendicular” to the plane are odd. The most prominent difference upon switching polarization occurs for the band, composed of d_{yz} orbitals in Fig. 2

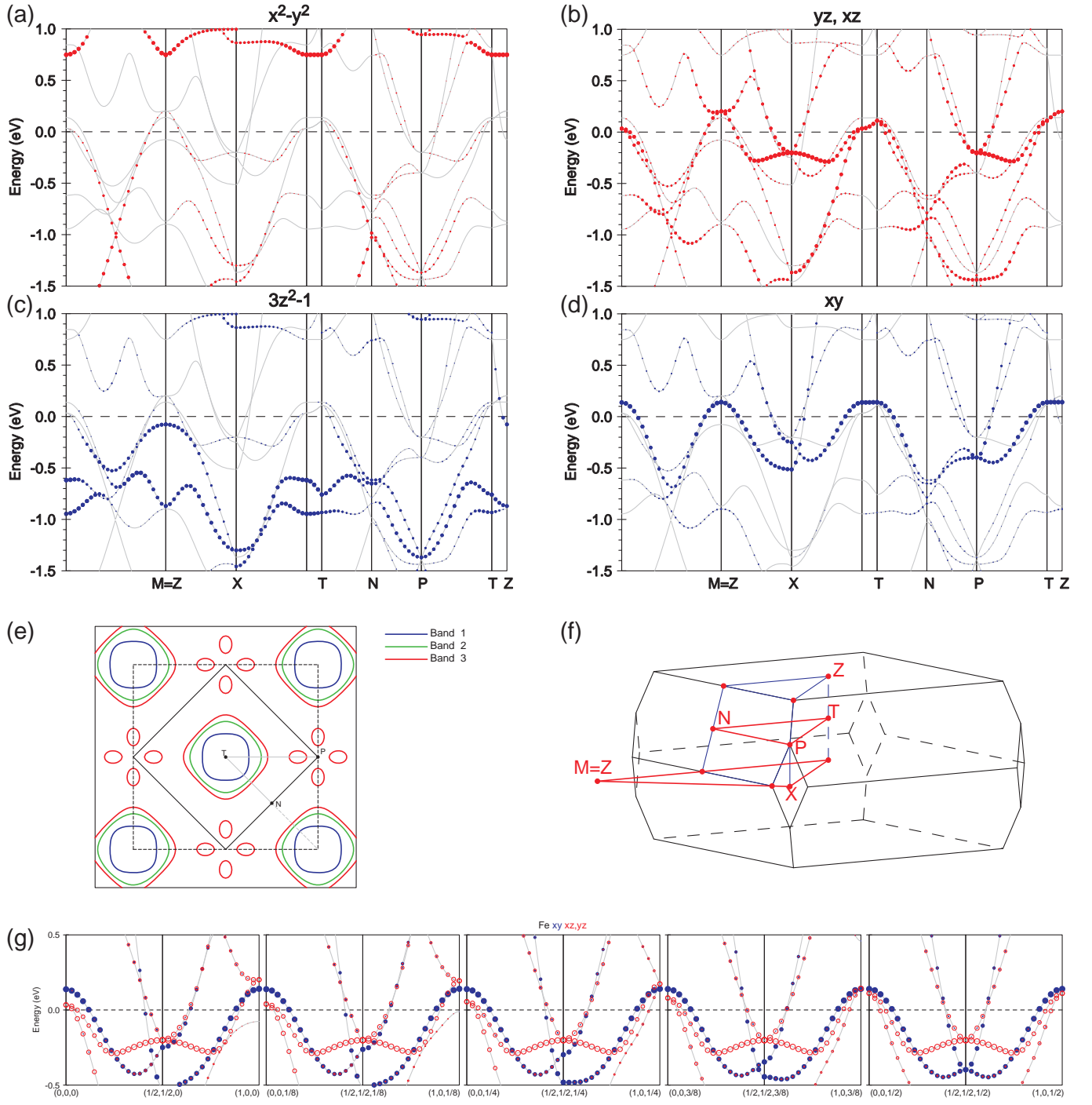


Fig. S3. Calculated band structure of BaFe_2As_2 . Panels (a,b,c,d) show the band dispersion and contribution from different iron 3d orbitals. (e) The calculated band dispersion cut at 250 meV below the Fermi level. (f) Three-dimensional Brillouin zone. (g) Band dispersion for different k_z values.

(for the orbital character, obtained from the calculation, see Fig. S3 and Fig. S3 (e) in Ref. 29).

It is still unclear, whether the entire propeller-shaped intensity, seen in ARPES (including central small electron-like pocket), can be satisfactory reproduced by cutting the calculated band structure at the suitable en-

ergy level and emulation of the self energy effects. Additionally, temperature dependence of ARPES signal from propellers has been observed [11, S6], suggesting that appearance of propeller bands at the Fermi level has a connection to the fluctuations of magnetic order. Still, looking at the orbital composition of the calculated bands in

this region [Fig. S3] and at the polarization dependence of ARPES spectra [Fig. 2(c,d)], together with calculated and experimental dispersions it seems very reasonable to suggest that all propeller constituents, i.e. both shaft and blades, are “assembled” of iron $3d_{xz,yz}$ orbitals.

D. Temperature dependence of the superconducting gap

In Fig. S4 we show the temperature dependence of the ARPES spectra for temperature range from above T_c down to 1 K. As one can see from Fig. S4 (a,b,c), spectral signatures of the superconducting gap — “beaks” at Fermi crossings in the energy-momentum cuts and coherence peak in the integrated spectrum — appear when cooling through T_c . These signatures are present for both outer and inner Γ -barrels, implying that both large gap on the inner Γ -barrel and the small gap on the outer Γ -barrel, open at T_c . As discussed in the next section of the Supplementary Materials, ARPES spectra of BKFA contain large contribution of a component with reduced superconducting gap, stemming from the surface layer. This component of the photoemission data is taken into account upon fitting the data [S7], and the magnitude of the reduced gap can be extracted separately. In Fig. S4 (c) are shown temperature dependencies for the gap magnitude on the outer Γ -barrel, two unresolved inner Γ -barrels and surface component of the inner Γ -barrels. Thus, both small gap on the outer Γ -barrel and large gap on the inner Γ -barrels emerge upon entering the superconducting state, and consequently are unambiguously related to the superconductivity.

Fig. S4 (e) shows the Fermi surface map of optimally doped $\text{Ba}_{1-x}\text{Na}_x\text{Fe}_2\text{As}_2$ with T_c of 34 K. As one can see, the Fermi surface of $\text{Ba}_{1-x}\text{Na}_x\text{Fe}_2\text{As}_2$ consists of hole-like Γ -barrels in the BZ center and propeller-like structure at the BZ corner, illustrating the already mentioned similarity of the electronic structures of sodium- and potassium-doped BaFe_2As_2 (see also Ref. S8). The temperature dependence of the cut, passing through the propeller’s blade [pink dashed line in panel (e)] is presented in Fig. S4 (f). The hole-like dispersion of the band, supporting propeller’s blades, is clearly visible. The development of the superconducting gap can be recognized as modification of the spectral function in the vicinity of the Fermi level in panel (f) and by growth of the prominent coherence peak in the integrated spectrum in panel (g). Clear observation of the large superconducting gap implies that the propeller-like Fermi surface takes active part in the superconductivity.

E. Additional component of the photoemission signal from the inner Γ -barrel

Already in first studies of the superconducting gap in BKFA an additional component of the inner Γ -barrel was

noticed and attributed to the non-superconducting part of the photoemission spectrum [25, 26]. More recent experiments have shown that this feature is not entirely non-superconducting, but bears a reduced superconducting gap of 3–7 meV [13, S9]. To investigate this issue more thoroughly we have performed time-dependent measurements of the intensity distribution in the vicinity of the Fermi level in the superconducting state. Fig. S5 (a–d) shows two equivalent spectra taken from the same cleaved sample surface soon after cleavage and on the next day. Aged sample surface obviously exhibits a prominent non-superconducting (or bearing very small gap) component, while for the fresh cleavage the secondary component is gapped with ~ 6 meV gap, and therefore, is not that prominent, merging visually with the peak from the ~ 11 meV gap. Interestingly, both in case of aged and fresh surfaces, the large gap remains the same, ~ 11 meV, i.e. is robust with respect to surface degradation. The inner Γ -barrel is double-walled, so generally one might expect an additional feature at this location in the Brillouin zone: each of these two nearly degenerate bands might bear different superconducting gaps. However, such explanation for two distinct gaps in this momentum region faces the following difficulties: (i) the two inner Γ -barrels are highly degenerate and have virtually the same orbital composition of the wave functions, therefore it seems unlikely that they bear such different gap magnitudes (6 vs. 10.5 meV), and (ii) one of the gaps almost completely vanishes with time, while the other remains unchanged, also implying different origin of the two neighboring features, while the impact of surface degradation on the two components of the inner Γ -barrel is expected to be very similar as they both are composed of the same iron $d_{xz,yz}$ -orbitals. A more plausible explanation is that the spectral feature with reduced gap is connected to the photoemission signal from the top-most surface layer, and consequently, should be filtered out when speaking of the bulk gap structure.

Fig. S5 (e,f) show two spectra, taken in the very same conditions from the same cleave even with no adjustment of sample position. The difference between these two spectra is due to surface degradation, related to the residual pressure in the measuring chamber. Visually presence of a component with reduced gap is seen as a “hat” on top of the feature bearing large gap [see Fig. S5 (c,f)]. The difference between spectra in panels (e) and (f) is that this hat is shifted more towards the Fermi level, i.e. further from the feature with the robust large gap. Panel (g) shows a detailed analysis of the near- k_F EDC from panels (e) and (f). The peak in the EDC is fitted to two Lorentzians, also shown in panel (g) below the data. Remarkably, the difference in the fits for more and less degraded spectra is only in the shift of the Lorentzian, located at the lower binding energy to even lower; at the same time the position of the Lorentzian at higher binding energy and relative weights of Lorentzians remain unchanged. This allows us to state that the main effect of surface degradation is in further closing of the reduced

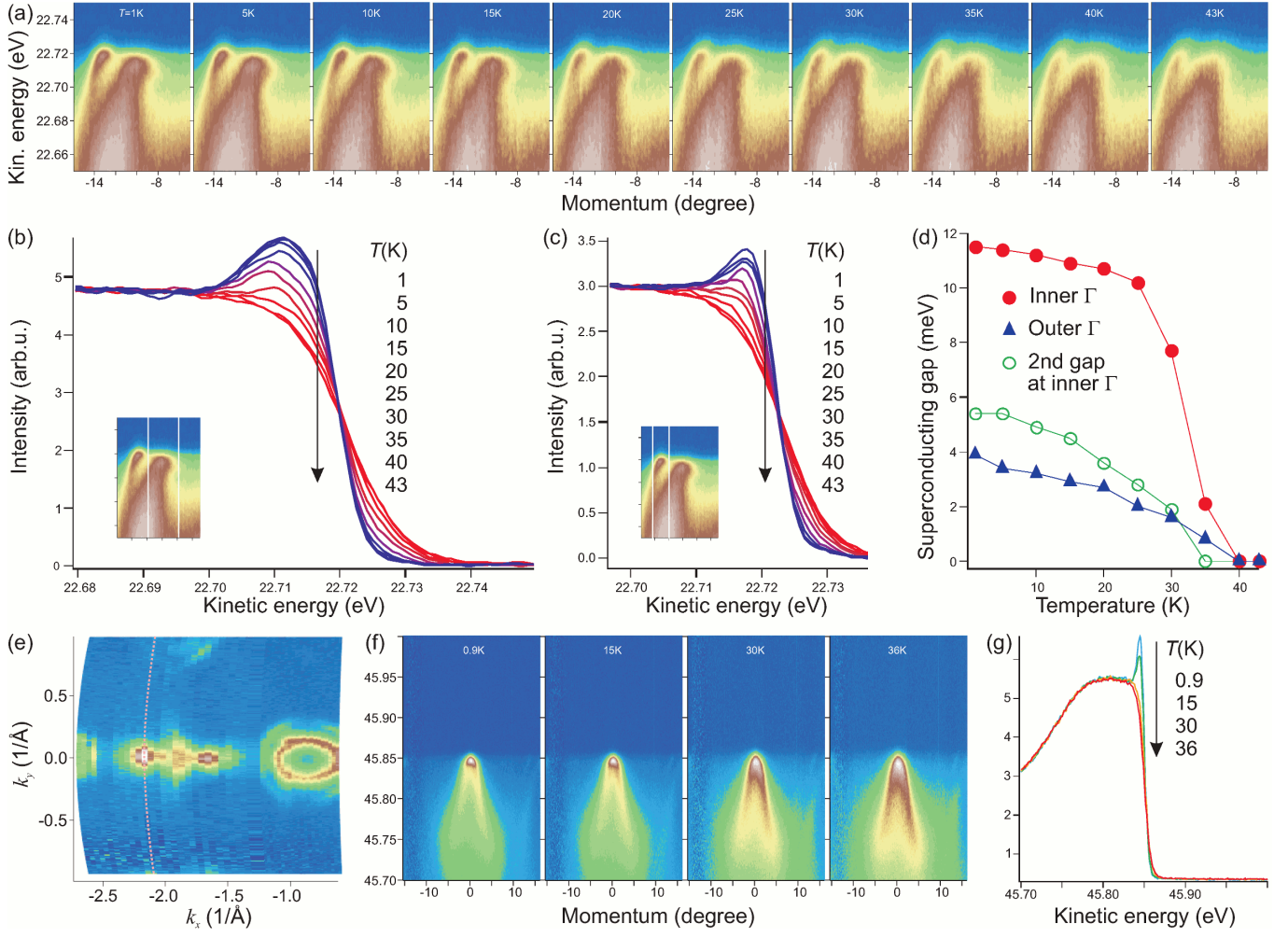


Fig. S4. (a) Sequence of temperature-dependent measurements, performed on $\text{Ba}_{1-x}\text{K}_x\text{Fe}_2\text{As}_2$ with T_c of 38 K, for the energy-momentum cut, passing through the Γ -barrels in the range of 1–43 K. The emergence of superconducting gap shows up as appearance of the “beaks” at Fermi crossings of both inner and outer Γ -barrels. (b) Temperature dependence of the EDC, referring to the inner Γ -barrel, integrated in the range shown in the inset. The spectrum above T_c is nothing but Fermi step, while the coherence peak starts to grow at superconductivity onset. (c) Same as (b), only for the outer Γ -barrel. (d) Temperature dependence of the superconducting gaps, derived from fit of integrated EDC to Dynes function. Panels (e,f,g) present data, taken from $\text{Ba}_{1-x}\text{Na}_x\text{Fe}_2\text{As}_2$ with $T_c = 34$ K. (e) Fermi surface map. (f) Temperature dependence of the energy-momentum cut passing through the center of the propeller’s blade, as shown by dashed line in panel (e). (g) Temperature dependence of the integrated EDC, revealing the appearance of prominent coherence peak below T_c .

gap.

To get some quantitative estimate of the residual pressure effect on the surface degradation, we have performed a time-dependent measurements of the same spectrum capturing Γ -barrels [Fig. S5 (h)]. The residual pressure was $1.3 \cdot 10^{-10}$ mbar, and time interval between consequent measurement, shown in panel (h), was 12.5 minutes. In the Fig. S5 (i) we plot the temperature dependence for positions of the leading edge midpoints of the inner and outer Γ -barrels. The time evolution for the inner Γ -barrel shows exponential behavior with time constant of approximately one hour. The same temperature dependence for the outer Γ -barrel shows small decrease instead of expected small increase due to onset of differ-

ent effects (variation of intensity distribution, broadening of spectral features etc.) influencing the leading edge midpoint position.

We emphasize once more that the large superconducting gap on the inner Γ -barrel, is a robust property of the ARPES spectra of optimally doped BKFA, while the reduced gap is strongly dependent on the experimental conditions, and most likely is related to the surface. It is worthwhile noting that in the case of ARPES experiments on LiFeAs no additional components of the signal with reduced gap has been noticed and the spectra generally deteriorate less with time passed after cleavage [15, S10]. The reason is that, in contrast to 122 iron arsenides, LiFeAs has a natural cleavage plain and topmost

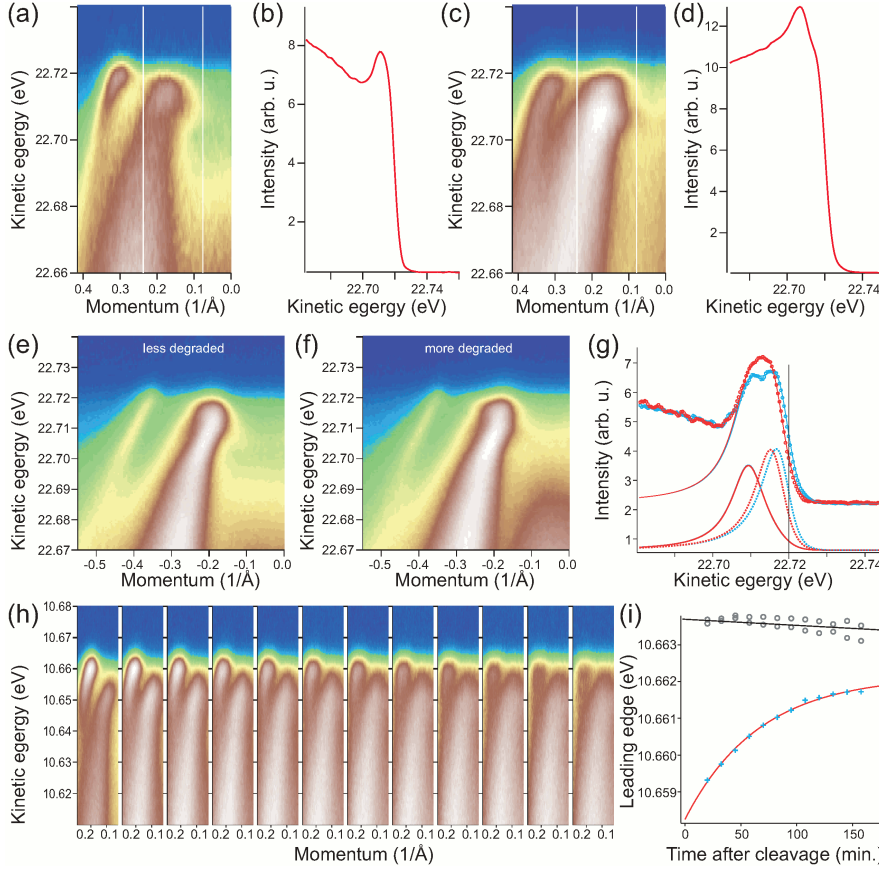


Fig. S5. Deterioration of the sample surface with time after cleavage results in reduction of the gap in surface-related part of the photoemission spectrum. At the same time another, bulk, component of the signal exhibits a robust time-independent gap value. (a) Energy-momentum cut, passing through the Γ -point, recorded soon after cleavage. (b) EDC, integrated around the Fermi crossing of the inner Γ -barrel, as indicated in the panel (a). (c) The same cut, recorded from the same cleave after more than 25 hours. (d) Corresponding EDC. (e,f,g) is a different data set, where (e) and (f) panels represent signals from less and more deteriorated surface respectively. (g) Near- k_F EDCs after deconvolution together with fits to two lorentzians. The peak, corresponding to bulk signal remains unchanged, while the peak, corresponding to the surface signal with reduced gap shifts towards Fermi level. (h) Third data set: time evolution of the similar cut, passing through the Γ -barrels, recorded immediately after cleavage at residue pressure in the measuring chamber of $1.3 \cdot 10^{-10}$ mbar and using Janis ST400 cryomanipulator. (i) Time dependence of the leading edge position (LEG) for the outer (grey circles) and inner (blue crosses) Γ -barrels.

superconducting Fe-As layer appears to be covered with a whole Li layer.

Presence of two components in the spectra—the one with a reduced gap value, dependent on the surface quality, and the other with large robust gap—imply that the observed spectra represent a sum of a signal coming from the topmost surface layer and a signal from the deeper subsurface layers. The fact that the difference between the surface and subsurface signal mainly consists in

the different gap values, while no difference in the band dispersion was detected, suggests that surface effects are not crucial for determination of the band dispersion from ARPES on $\text{Ba}_{1-x}\text{K}_x\text{Fe}_2\text{As}_2$. Together with matching Hall measurements [S6] and with opening of the large superconducting gap at propellers [Fig. S4 (f)], it gives good substantiation for the bulk origin of the propeller-like Fermi surface. Large superconducting gap opening at propeller implies active role in superconductivity.

- [S1] D. S. Inosov, R. Schuster, A. A. Kordyuk, J. Fink, S. V. Borisenko, V. B. Zabolotnyy, D. V. Evtushinsky, M. Knupfer, B. Büchner, R. Follath, and H. Berger, *Phys. Rev. B* **77**, 212504 (2008).
- [S2] S. Hüfner, *Photoelectron Spectroscopy* (Springer-Verlag, Berlin, 1996).
- [S3] V. B. Zabolotnyy, D. V. Evtushinsky, A. A. Kordyuk, D. S. Inosov, A. Koitzsch, A. V. Boris, G. L. Sun, C. T. Lin, M. Knupfer, B. Büchner, A. Varykhalov, R. Follath, S. V. Borisenko, *Physica C* **469**, 448 (2009).
- [S4] T. Yoshida, I. Nishi, A. Fujimori, M. Yi, R. G. Moore, D.-H. Lu, Z.-X. Shen, K. Kihou, P. M. Shirage, H. Kito, C. H. Lee, A. Iyo, H. Eisaki, H. Harima, *J. Phys. Chem. Sol.* **72**, 465 (2011).
- [S5] The fitting curves, used for approximation of the excita-

- tion energy dependence of the superconducting gap magnitudes on the Γ -barrels in Fig. 1 (d), are $\Delta_{\text{large}}(h\nu) = 10.5 - 5 \cdot \sin^8(0.5 \cdot 6.7 \cdot \sqrt{0.262 \cdot (h\nu + 7.6)})$, $\Delta'_{\text{large}}(h\nu) = 10.5 - 6 \cdot \sin^8(0.5 \cdot 6.7 \cdot \sqrt{0.262 \cdot (h\nu + 7.6)})$, $\Delta_{\text{small}}(h\nu) = 3.5$. Apart from the value of 7.6 eV for the inner potential, from fitting of the data we can infer that the peculiar points in the $h\nu$ dependence correspond to the $k_z = \pi$, i.e. Z point in the three-dimensional BZ. The deviation of the model from experimental data at photon energies below 20 eV is expected from break down of the free electron approximation for the final state.
- [S6] D. V. Evtushinsky, A. A. Kordyuk, V. B. Zabolotnyy, D. S. Inosov, Timur K. Kim, B. Büchner, H. Q. Luo, Z. S. Wang, H.-H. Wen, G. L. Sun, C. T. Lin, S. V. Borisenko, *J. Phys. Soc. Jpn.* **80**, 023710 (2011).

- [S7] Though the shape of the spectrum below T_c exhibits significant deviations from the BCS behavior, in particular due to prominent effects of a mode scattering [23], [P. Richard *et al.* Phys. Rev. Lett. **102**, 047003 (2009)] the values of the gap, extracted from the fit of the data to the Dynes function are still reasonable quantitative characteristics of the superconducting state. More detailed investigation of the spectrum shape is the matter of future studies.
- [S8] S. Aswartham, M. Abdel-Hafiez, D. Bombor, M. Kumar, A. U. B. Wolter, C. Hess, D. V. Evtushinsky, V. B. Zabolotnyy, A. A. Kordyuk, T. K. Kim, S. V. Borisenko, G. Behr, B. Büchner, S. Wurmehl, arXiv:1203.0143
- [S9] T. Shimojima, F. Sakaguchi, K. Ishizaka, Y. Ishida, T. Kiss, M. Okawa, T. Togashi, C.-T. Chen, S. Watanabe, M. Arita, K. Shimada, H. Namatame, M. Taniguchi, K. Ohgushi, S. Kasahara, T. Terashima, T. Shibauchi, Y. Matsuda, A. Chainani, and S. Shin, “Orbital-Independent Superconducting Gaps in Iron Pnictides”, Science **332**, 564 (2011).
- [S10] D. S. Inosov, J. S. White, D. V. Evtushinsky, I. V. Morozov, A. Cameron, U. Stockert, V. B. Zabolotnyy, T. K. Kim, A. A. Kordyuk, S. V. Borisenko, E. M. Forgan, R. Klingeler, J. T. Park, S. Wurmehl, A. N. Vasiliev, G. Behr, C. D. Dewhurst, and V. Hinkov, Phys. Rev. Lett. **104**, 187001 (2010).